Kuwait J. Sci. **43 (3)** pp. 1-13, 2016

Mixed convection flow of Powell-Eyring fluid over a stretching cylinder with Newtonian heating

Hafiz A. Wahab[1,*], Sajjad Hussain[1], Saira Bhatti[2], Muhammad Naeem[3]

[1]*Dept. of Mathematics, Hazara University Mansehra, Pakistan*

[2]*Dept. of Mathematics, CIIT Abbottabad, Pakistan*

[3]*Dept. of IT, Abbottabad University of Science & Technology, Abbottabad, Pakistan*

[*]*Corresponding author: wahabmaths@yahoo.com, wahab@hu.edu.pk*

Abstract

The aim of this article is to analyze the mixed convection flow of Powell-Eyring fluid induced by inclined stretching cylinder. Heat transfer analysis is subjected to the Newtonian heating and heat generation/absorption. A system of nonlinear partial differential equations is converted to a system of ordinary differential equations by suitable transformations. The series solution of the present problem is solved by homotopy analysis method. Behaviors of various parameters on skin friction coefficient, Nusselt number, velocity and temperature profiles are discussed. A comparison of skin friction coefficient for viscous and Powell-Eyring fluids with the previous existing data is also presented.

Keywords: Mixed convection; nNewtonian heating; Powell-Eyring fluid; stretching cylinder.

2000 Mathematics Subject Classification: 76A05; 76D05; 35Q35

1. Introduction

Rheological behaviors of non-Newtonian fluids are more complicated than the Newtonian fluids. Non-Newtonian fluids cannot be analyzed by a single constitutive equation due to their diverse and complex characteristics. In non-Newtonian fluids, there is a nonlinear relationship between the stress and the rate of strain. The governing equations of the non-Newtonian fluids are highly nonlinear and more complicated than the Newtonian fluids. In recent times researchers and scientists are interested in the study of non-Newtonian fluids due to their higher importance in many biological, industrial and engineering processes such as glass formation, fiber sheet manufacturing, wire drawing, food products, paper production, crystal growth etc. Examples of such non-Newtonian fluids are yoghurt, pasta, shampoo, mud, clay coatings, greases, certain oils, paints, ketchup etc. Powell-Eyring fluid model is one of the non-Newtonian fluid model which was first introduced by Powell and Eyring in 1944. This fluid model is very complex, but it attains the attention of the researchers and scientists due to its important applications and advantages. Firstly it is derived from kinetic theory of liquid, rather than the empirical relation. Secondly, it exhibits correctly to the Newtonian behavior for both low and high shear stresses. Khader & Megahed (2013) investigated the unsteady boundary layer flow of Powell-Eyring fluid over a stretching sheet with the effect of heat generation. Jalil & Asghar (2013) examined the heat transfer of Powell-Eyring fluid induced by stretching surface. Hayat *et al*. (2013) explored the boundary layer stagnation point flow of Powell-Eyring fluid with melting phenomenon. Magnetohydrodynamic convective flow of non-Newtonian Powell-Eyring fluid past a vertical plate saturated with porous medium is presented by Eldabe *et al.* (2012). The analysis of non-Newtonian Powell-Eyring fluid induced by stretching sheet is studied by Javed *et al*. (2013). Malik *et al*. (2013) presented the effects of variable viscosity in the flow of Powell-Eyring fluid past a stretching cylinder. Ara *et al*. (2014) presented the boundary layer flow of Powell-Eyring fluid over an exponentially shrinking sheet with radiation effects.

The characteristics of mixed convection flow are very important due to their vast applications in industrial, engineering and natural processes. Mixed convection is the combination of natural and forced convection. Currently, the analysis of aerosol deposition is very significant in the engineering processes. Specifically, the contaminant particle deposition onto the surface of products in the electronic industry has a pivotal role regarding the quality of manufactured product. Convection is one of the important

factors that greatly influence the particle deposition. Mixed convection flows are encountered in many engineering and industrial applications. Such phenomenon is encountered in solar energy systems, nuclear reactors cooling during emergency shutdown, cooling of electronic devices, boilers, cooling of combustion chamber wall in a gas turbine, defroster system, automobile demister and flows in the atmosphere and ocean. Ferdows *et al*. (2012) investigated the MHD mixed convective flow of nanofluid due to an exponentially stretching plate. Srinivasacharya & Surender (2014) examined the mixed convection flow of a nanofluid over a vertical plate in a porous medium with double stratification. The effect of heat source/sink on MHD mixed convection flow of nanofluid on a vertical sheet with suction or injection is studied by Keshtkar *et al*. (2014). Li *et al*. (2011) explored the mixed convection stagnation-point flow of a viscoelastic fluid over a vertical sheet. Hayat *et al*. (2014) presented the mixed convection flow of viscoelastic fluid with thermal radiations and convective conditions.

Merkin (1994) pointed out that wall to ambient temperature distribution is encountered by four common processes of heat transfer namely (i) constant or prescribed surface temperature, (ii) constant or prescribed surface heat flux, (iii) conjugate boundary conditions and (iv) Newtonian heating in which heat transfer from bounding surface with a finite heat capacity is proportional to the local surface temperature. In recent developments, the Newtonian heating processes have been used by various researchers due to their wide range of applications such as the designing of conjugate heat transfer around fins, heat exchanger and in the setup of convection flows in which bounding surfaces absorb heat by solar radiations. The effect of Newtonian heating in the flow of nanofluid with viscous dissipation is studied by Makinde (2013). Sarif *et al*. (2013) explored boundary layer flow past a stretching sheet with Newtonian heating. Makinde (2012) examined the effects of Newtonian and Navier slip in the MHD flow over a flat plate. The effect of Newtonian heating on MHD free convective flow of a nanofluid over a flat vertical surface is investigated by Uddin *et al*. (2012). Narahari & Dutta (2012) studied the effects of mass diffusion and thermal radiations on free convection flow near a vertical surface with Newtonian heating.

Recently the researchers and scientists are interested to reduce the skin friction coefficient and enhance the rate of heating or cooling in the advanced technological processes. Thus various attempts have been made about the reduction of skin friction or drag forces for flows over the surface of a wing, tail plane and wind turbine rotor etc. However these forces can be reduced by keeping the boundary layer away from separation and to delay the transition of laminar to turbulent flow. This task can be performed through different physical aspects such as moving the surface, through fluid suction and injection and the presence of body forces. Similarly most of the researchers have been tried to enhance the rate of cooling/heating by using different types of boundary conditions over a flat plate. So our main objective is to overcome such difficulties by studying mixed convection flow of Powell-Eyring fluid over an impermeable inclined stretching cylinder (instead of a stretching flat plate) with Newtonian heating. The flow analysis is carried out over an inclined stretching cylinder, while the resulting nonlinear equations are solved by homotopy analysis method (Rashidi *et al*., 2012; Abbasbandy *et al*., 2013; Hassan & Rashidi, 2013; Liao, 2012; Turkyilmazoglu, 2012) representing convergent series solutions with various numerical values of the skin friction coefficient and Nusselt number.

2. Mathematical formulation

Consider the steady, two dimensional and incompressible mixed convection flow of Powell-Eyring fluid over an inclined stretching cylinder of radius R. Newtonian heating and heat generation/absorption effects are also incorporated. The x-axis is taken along the axial direction of cylinder while the r-axis is normal to it. The physical model and coordinate system of the problem are shown in Figure 1. Two forces which are equal in magnitude but opposite in direction are applied to the cylinder such that origin is kept fixed. Using the boundary layer approximations, the governing equations take the forms;

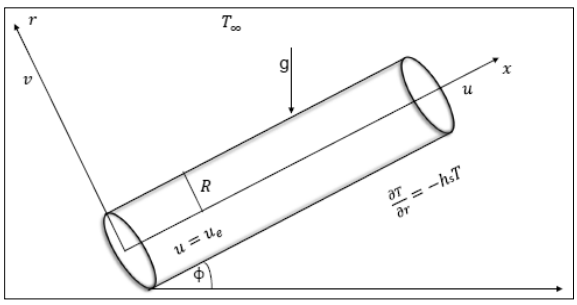

Fig. 1. Physical model and the coordinate system.

$$\frac{\partial (ru)}{\partial x} + \frac{\partial (rv)}{\partial r} = 0, \tag{1}$$

$$u\frac{\partial u}{\partial x}+v\frac{\partial u}{\partial r}=\nu\left(\frac{\partial^2 u}{\partial r^2}+\frac{1}{r}\frac{\partial u}{\partial r}\right)+\frac{1}{\rho\beta c}\left(\frac{\partial^2 u}{\partial r^2}+\frac{1}{r}\frac{\partial u}{\partial r}\right)$$
$$-\frac{1}{6\rho\beta c^3}\left(\frac{1}{r}\left(\frac{\partial u}{\partial r}\right)^3+3\left(\frac{\partial u}{\partial r}\right)^2\left(\frac{\partial^2 u}{\partial r^2}\right)\right)+g\beta_T\left(T-T_\infty\right)\sin\varphi, \quad (2)$$

$$u\frac{\partial T}{\partial x}+v\frac{\partial T}{\partial r}=\frac{k}{\rho c_p}\left(\frac{\partial^2 T}{\partial r^2}+\frac{1}{r}\frac{\partial T}{\partial r}\right)+\frac{Q_\circ}{\rho c_p}\left(T-T_\infty\right), \quad (3)$$

The relevant boundary conditions are

$$u=u_e=\frac{U_\circ x}{l},\ v=0,\ \frac{\partial T}{\partial r}=-h_s T \ \text{ at } r=R,$$
$$u\to 0,\ T\to T_\infty \ \text{ as } r\to\infty, \quad (4)$$

In above equations u indicates the velocity component along x-axis and v indicates the velocity component along r-axis, ρ is the density, φ is the angle of inclination, T is the temperature of fluid, $\nu=\left(\frac{\mu}{\rho}\right)$ the kinematic viscosity, g is the gravity, β_T is the coefficient of thermal expansion, T_∞ is the ambient fluid temperature, β and c are the fluid parameters, u_e is the stretching velocity, $U_\circ$ is the reference velocity, $Q_\circ$ is the heat generation/absorption coefficient, h_s is the heat transfer coefficient and l is the characteristic length.

$$\eta=\sqrt{\frac{U_\circ}{\nu l}}\left(\frac{r^2-R^2}{2R}\right),\ u=\frac{U_\circ x}{l}f'(\eta),$$
$$v=-\sqrt{\frac{\nu U_\circ}{l}}\frac{R}{r}f(\eta),\ \theta(\eta)=\frac{T-T_\infty}{T_\infty}, \quad (5)$$

Using the following transformations

The equation (1) is identically satisfied while Equations (2) and (3) reduce to the following forms

$$(1+M)(1+2\eta\gamma)f'''-\alpha M(1+2\eta\gamma)^2 f''^2 f'''$$
$$+2\gamma(1+M)f''+ff''$$
$$-\frac{4}{3}\alpha M\left(\gamma+2\eta\gamma^2\right)f'''^3-f'^2+\lambda\theta\sin\varphi=0, \quad (6)$$

$$(1+2\eta\gamma)\theta''+2\gamma\theta'+\Pr f\theta'+\Pr\delta\theta=0, \quad (7)$$

with the following boundary conditions,

$$f(0)=0, f'(0)=1,\ \theta'(0)=-\sigma\left(1+\theta(0)\right),$$
$$f'(\eta)\to 0,\ \theta(\eta)\to 0 \text{ as } \eta\to\infty. \quad (8)$$

Here γ is the curvature parameter, α and M are the fluid parameters, λ is the mixed convection parameter, Pr is the Prandtl number, δ is the heat generation/absorption parameter and σ is the conjugate parameter.

$$\alpha=\frac{U_\circ^3 x^2}{2l^3c^2\nu},\ \gamma=R^{-1}\left(\frac{\nu l}{U_\circ}\right)^{\frac{1}{2}},\ M=\frac{1}{\mu\beta c},\ \Pr=\frac{\nu\rho c_p}{k},$$
$$\lambda=\frac{l^2 g\beta_T}{U_\circ^2 x}T_\infty,\ \delta=\frac{Q_\circ l}{\rho c_p U_\circ},\ \sigma=h_s\left(\frac{\nu l}{U_\circ}\right)^{\frac{1}{2}}, \quad (9)$$

The skin friction coefficient C_f and local Nusselt number Nu_x are the physical quantities of interest, which are defined as

$$C_f=\frac{\tau_w}{\rho u_e^2},\quad Nu_x=\frac{xq_w}{k\left(T-T_\infty\right)}, \quad (10)$$

$$\tau_w=\left[\left(\mu+\frac{1}{\beta c}\right)\frac{\partial u}{\partial r}-\frac{1}{6\beta c^3}\left(\frac{\partial u}{\partial r}\right)^3\right]_{r=R},\ q_w=-k\left(\frac{\partial T}{\partial r}\right)_{r=R}. \quad (11)$$

where τ_w and q_w are the surface shear stress and surface heat flux respectively. In dimensionless forms we have

$$\mathrm{Re}_x^{\frac{1}{2}}C_f=(1+M)f''(0)-\frac{\alpha}{3}Mf'''^3(0),$$
$$\frac{Nu_x}{\mathrm{Re}_x^{\frac{1}{2}}}=\sigma\left(\frac{1}{\theta(0)}+1\right). \quad (12)$$

where $\mathrm{Re}_x=\frac{U_\circ x^2}{\nu l}$ is the local Reynolds number (ratio of inertial forces to viscous forces).

3. Series solutions by ham

To find the series solution for the highly non-linear ordinary differential equations by homotopy analysis method, we choose the following initial approximations and auxiliary linear operators

$$f_0(\eta)=1-\exp(-\eta),\quad \theta_0(\eta)=\frac{\sigma\exp(-\eta)}{1-\sigma}, \quad (13)$$

$$\mathcal{L}_f=f'''-f',\quad \mathcal{L}_\theta=\theta''-\theta, \quad (14)$$

$$\mathcal{L}_f\left[E_1+E_2\exp(-\eta)+E_3\exp(\eta)\right]=0, \quad (15)$$

$$\mathcal{L}_\theta\left[E_4\exp(-\eta)+E_5\exp(\eta)\right]=0, \quad (16)$$

where $E_j\ (j=1\ to\ 5)$ are the arbitrary constants.

3.1. Zeroth order approximation

Expressing the zeroth order problem as

$$(1-q)\mathcal{L}_f\left[\bar{f}(\eta;q)-f_0(\eta)\right]=q\hbar_f N_f\left[\bar{f}(\eta;q),\bar{\theta}(\eta;q)\right], \quad (17)$$

with

$$\bar{f}(0;q)=0,\ \ \bar{f}'(0;q)=1,\ \ \bar{f}'(\infty;q)=0, \quad (18)$$

$$(1-q)\mathcal{L}_\theta\left[\bar{\theta}(\eta;q)-\theta_0(\eta)\right]=q\hbar_\theta N_\theta\left[\bar{f}(\eta;q),\bar{\theta}(\eta;q)\right], \quad (19)$$

with

$$\bar{\theta}'(0;q)=-\sigma\left[1+\bar{\theta}(0;q)\right],\ \ \bar{\theta}(\infty;q)=0, \quad (20)$$

In above equations $\hbar_f$, $\hbar_\theta$ and $q\in[0,1]$ are the non-zero auxiliary parameters and the embedding parameter respectively, whereas the non-linear operators N_f and N_θ are defined as

$$\begin{aligned}N_f\left[\bar{f}(\eta;q),\bar{\theta}(\eta;q)\right]&=(1+M)(1+2\eta\gamma)\frac{\partial^3\bar{f}(\eta;q)}{\partial\eta^3}+2\gamma(1+M)\frac{\partial^2\bar{f}(\eta;q)}{\partial\eta^2}\\&-\alpha M(1+2\eta\gamma)^2\left(\frac{\partial^2\bar{f}(\eta;q)}{\partial\eta^2}\right)^2\frac{\partial^3\bar{f}(\eta;q)}{\partial\eta^3}+\bar{f}(\eta;q)\frac{\partial^2\bar{f}(\eta;q)}{\partial\eta^2}\\&-\frac{4}{3}\alpha M\left(\gamma+2\eta\gamma^2\right)\left(\frac{\partial^2\bar{f}(\eta;q)}{\partial\eta^2}\right)^3-\left(\frac{\partial\bar{f}(\eta;q)}{\partial\eta}\right)^2+\lambda\bar{\theta}(\eta;q)\sin\varphi,\end{aligned} \quad (21)$$

$$\begin{aligned}N_\theta\left[\bar{f}(\eta;q),\bar{\theta}(\eta;q)\right]&=(1+2\eta\gamma)\frac{\partial^2\bar{\theta}(\eta;q)}{\partial\eta^2}+2\gamma\frac{\partial\bar{\theta}(\eta;q)}{\partial\eta}\\&+\Pr\bar{f}(\eta;q)\frac{\partial\bar{\theta}(\eta;q)}{\partial\eta}+\Pr\delta\bar{\theta}(\eta;q),\end{aligned} \quad (22)$$

putting $q=0$ and $q=1$ then we have

$$\bar{f}(\eta;0)=f_0(\eta),\ \ \bar{f}(\eta;1)=f(\eta), \quad (23)$$

$$\bar{\theta}(\eta;0)=\theta_0(\eta),\ \ \bar{\theta}(\eta;1)=\theta(\eta), \quad (24)$$

With the variation of q from 0 to 1, $\bar{f}(\eta;q)$ and $\bar{\theta}(\eta;q)$ vary continuously from initial approximations $f_0(\eta)$ and $\theta_0(\eta)$ to the exact solutions $f(\eta)$ and $\theta(\eta)$ respectively. By Taylor's series we obtain,

$$\bar{f}(\eta;q)=f_0(\eta)+\sum_{n=1}^{\infty}f_n(\eta)q^n;\ \ \text{where } f_n(\eta)=\frac{1}{n!}\frac{\partial^n\bar{f}(\eta;q)}{\partial q^n}\Big|_{q=0}, \quad (25)$$

$$\bar{\theta}(\eta;q)=\theta_0(\eta)+\sum_{n=1}^{\infty}\theta_n(\eta)q^n;\ \ \text{where } \theta_n(\eta)=\frac{1}{n!}\frac{\partial^n\bar{\theta}(\eta;q)}{\partial q^n}\Big|_{q=0}, \quad (26)$$

Selecting $\hbar_f$ and $\hbar_\theta$ so precisely that at $q=1$, Equations (25) and (26) converge to the exact solution, i.e.

$$f(\eta)=f_0(\eta)+\sum_{n=1}^{\infty}f_n(\eta),\ \ \theta(\eta)=\theta_0(\eta)+\sum_{n=1}^{\infty}\theta_n(\eta), \quad (27)$$

3.2. *n*th-order deformation problems

$$\mathcal{L}_f\left[f_n(\eta)-\chi_n f_{n-1}(\eta)\right]=\hbar_f R_n^f(\eta), \quad (28)$$

$$\mathcal{L}_\theta\left[\theta_n(\eta)-\chi_n\theta_{n-1}(\eta)\right]=\hbar_\theta R_n^\theta(\eta), \quad (29)$$

$$f_n(0)=f_n'(0)=f_n'(\infty)=0, \quad (30)$$

$$\theta_n'(0)+\sigma\theta_n(0)=\theta_n(\infty)=0, \quad (31)$$

$$R_n^f(\eta)=(1+M)(1+2\eta\gamma)f_{n-1}'''-\alpha M(1+2\eta\gamma)^2\sum_{j=0}^{n-1}f_{n-1-j}''\sum_{k=0}^{j}f_{j-k}''f_k'''$$
$$+2\gamma(1+M)f_{n-1}''-\frac{4}{3}\alpha M\left(\gamma+2\eta\gamma^2\right)\sum_{j=0}^{n-1}f_{n-1-j}''\sum_{k=0}^{j}f_{j-k}''f_k'' \quad (32)$$
$$+\sum_{j=0}^{n-1}f_{n-1-j}f_j''-\sum_{j=0}^{n-1}f_{n-1-j}'f_j'+\lambda\theta_{n-1}\sin\varphi,$$

$$R_n^\theta(\eta)=(1+2\eta\gamma)\theta_{n-1}''+2\gamma\theta_{n-1}'+\Pr\sum_{j=0}^{n-1}\theta_{n-1-j}'f_j+\Pr\delta\theta_{n-1}, \quad (33)$$

$$\chi_n=\begin{cases}0, & n\le 1\\ 1, & n>1\end{cases} \quad (34)$$

The general solutions (f_n,θ_n) of Equations (28) and (29) can be expressed in terms of special solutions $\left(f_n^\bullet,\theta_n^\bullet\right)$ as

$$f_n(\eta)=f_n^\bullet(\eta)+E_1+E_2\exp(-\eta)+E_3\exp(\eta). \quad (35)$$

$$\theta_n(\eta)=\theta_n^\bullet(\eta)+E_4\exp(-\eta)+E_5\exp(\eta). \quad (36)$$

where the values of $E_j\,(j=1\ to\ 5)$ with the boundary conditions (30) and (31) are

$$E_3=E_5=0,\ E_2=\frac{\partial f_n^\bullet(\eta)}{\partial\eta}\Big|_{\eta=0},\ E_1=-E_2-f_n^\bullet(0),$$
$$E_4=\frac{1}{1-\sigma}\left[\theta_n^{\bullet\prime}(\eta)\big|_{\eta=0}+\sigma\theta_n^\bullet(\eta)\big|_{\eta=0}\right]. \quad (37)$$

3.3. Convergence analysis

As we know that the derived homotopic solutions have the auxiliary parameters $\hbar_f$ and $\hbar_\theta$. For proper range of auxiliary parameters, the $\hbar-$ curves are sketched at $17th$ order of approximations to ensure the convergence of the solutions. It is obvious from Figures 2 and 3 that the meaningful values of $\hbar_f$ and $\hbar_\theta$ are $-0.78\le\hbar_f\le-0.29$ and $-1.1\le\hbar_\theta\le-0.07$.

4. Results and discussion

The aim of this section is to discuss the behavior of various parameters on velocity and temperature profiles. Figure 4 shows the behavior of fluid parameter M on the velocity profile. The velocity and boundary layer thickness increase for higher values of fluid parameter M. Figure 5 is plotted for the effect of fluid parameter M on temperature profile. It is observed that temperature and thermal boundary layer thickness decrease with an increase in M. The influence of fluid parameter α on velocity and temperature profiles are sketched in Figures 6 and 7. It is noted that velocity and temperature profiles have opposite behavior with the fluid parameter α. Figure 8 shows the influence of heat generation parameter δ on velocity profile. The velocity and boundary layer thickness increase with an increase in δ. Figure 9 presents the behavior of heat generation parameter δ on temperature profile. It is depicted that the temperature and thermal boundary layer thickness are higher for larger values of heat generation parameter. Because heat generation coefficient increases, which is responsible for the enhancement of temperature profile. The influence of curvature parameter γ on velocity profile is displayed in Figure 10. It is observed that velocity profile decreases, near the surface which increases away from the surface for higher values of curvature parameter, because with the increase in curvature parameter, the radius of cylinder decreases. So contact area of the cylinder with the fluid decreases, which offers less resistance to the fluid motion so that the velocity profile increases. Figure 11 is displayed for the behavior of curvature parameter γ on temperature profile. For higher values of curvature parameter, the temperature profile decreases near the surface of cylinder while increases away from the surface. The influence of mixed convection parameter λ on velocity profile is sketched in Figure 12. The velocity and boundary layer thickness increase for higher values of mixed convection parameter. Because with the increase in mixed convection parameter, buoyancy force increases which is responsible for the enhancement of velocity profile. Figure 13 is plotted for the effect of mixed convection parameter λ on temperature profile. It is noted that temperature and thermal boundary layer thickness are higher for small values of mixed convection parameter. Because the rate of heat increases for higher values mixed convection parameter, which results in the reduction of temperature profile. Effect of angle of inclination φ on velocity profile is plotted in Figure 14. The velocity profile increases with an increase in angle of inclination. It is due to the fact that buoyancy force increases with angle φ. Therefore velocity profile increases. Influence of angle φ on temperature profile is shown in Figure.

15. Temperature profile decreases for high angle φ. Also thermal boundary layer thickness decreases. Behavior of Prandtl number Pr on velocity profile is shown in Figure 16. It is analyzed that velocity and momentum boundary layer thickness decrease when Pr increases. Because higher Prandtl number corresponds to higher momentum diffusivity which decreases the velocity profile. Figure 17 displays the influence of Prandtl number on temperature profile. It is depicted that temperature and thermal boundary layer thickness decrease for higher Prandtl number. Because thermal diffusivity decreases for larger Pr, which results in the reduction of temperature profile. Characteristics of conjugate parameter σ on velocity and temperature profiles are sketched in Figures. 18 and 19. It is analyzed that velocity and temperature profiles increase with an increase in conjugate parameter. Because heat transfer coefficient increases with an increase in conjugate parameter. Therefore, temperature profile increases.

Table 1 shows the convergence analysis of the series solutions. It is noted that 15*th* and 23*rd* order of approximations are sufficient for the convergence of $f''(0)$ and $\theta'(0)$ respectively. Table 2 presents the behavior of different parameters on skin friction coefficient and Nusselt number. It is noted that skin friction coefficient increases with γ, M and Pr while it decreases with α, λ, φ , δ and σ. Nusselt number increases for higher values of γ, M, λ, φ, Pr and σ while it decreases with α and δ. Tables 3 and 4 show the comparisons of $f''(0)$ and skin friction coefficient with the previous results. It is examined that all the results are in good agreement.

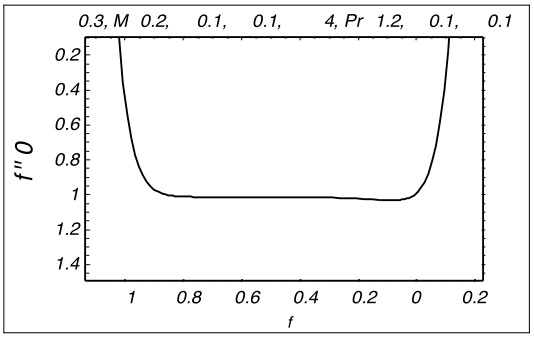

Fig. 2. $\hbar$ − curve for $f(\eta)$

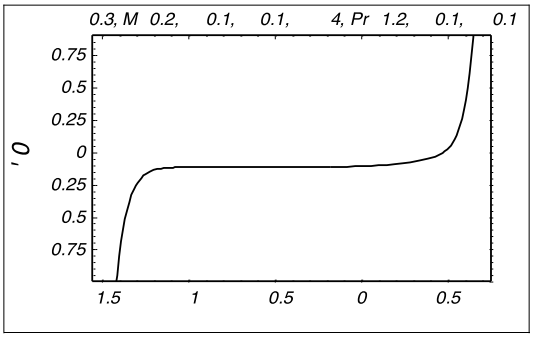

Fig. 3. $\hbar$ − curve for $\theta(\eta)$

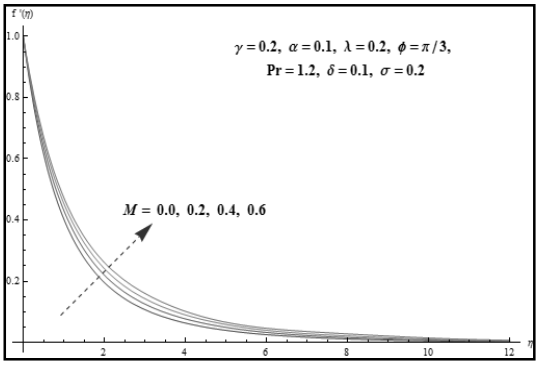

Fig. 4. Effect of M on $f'(\eta)$

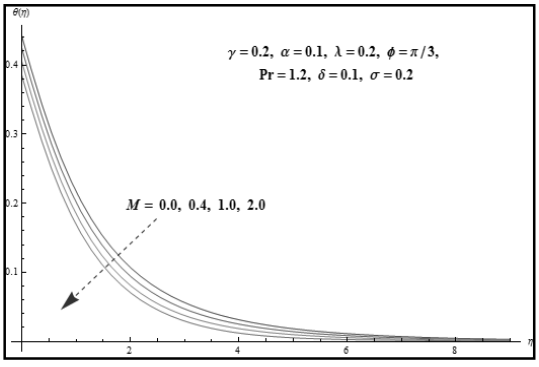

Fig. 5. Effect of M on $\theta(\eta)$

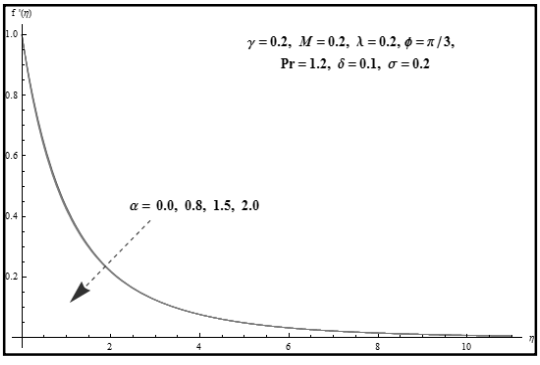

Fig. 6. Effect of α on $f'(\eta)$

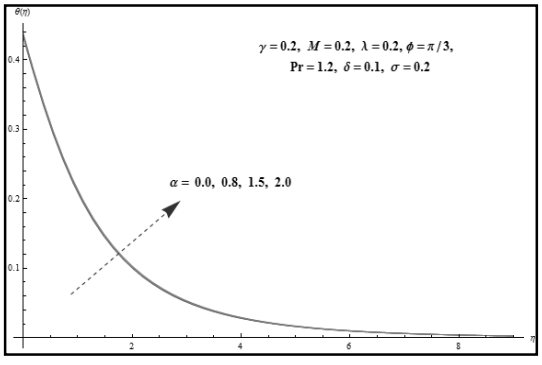

Fig. 7. Effect of α on $\theta(\eta)$

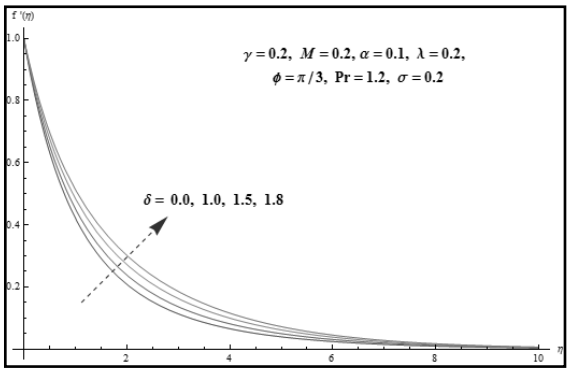

Fig. 8. Effect of δ on $f'(\eta)$

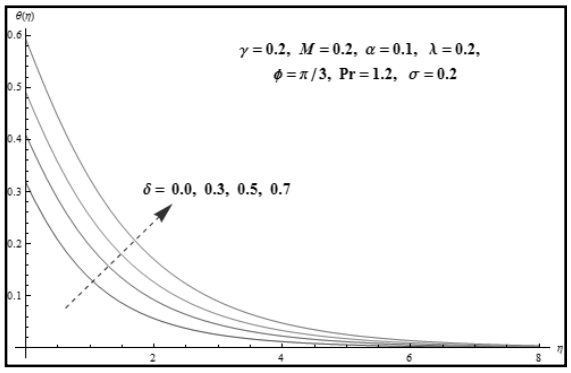

Fig. 9. Effect of δ on $\theta(\eta)$

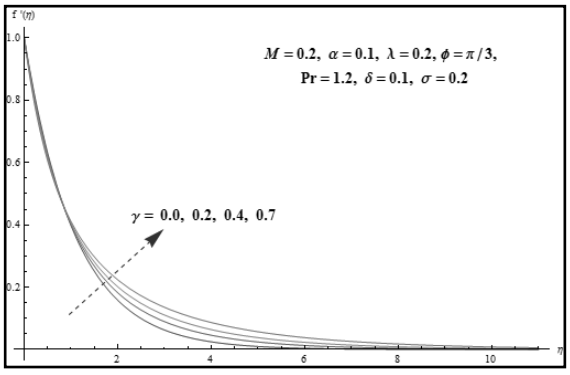

Fig. 10. Effect of γ on $f'(\eta)$

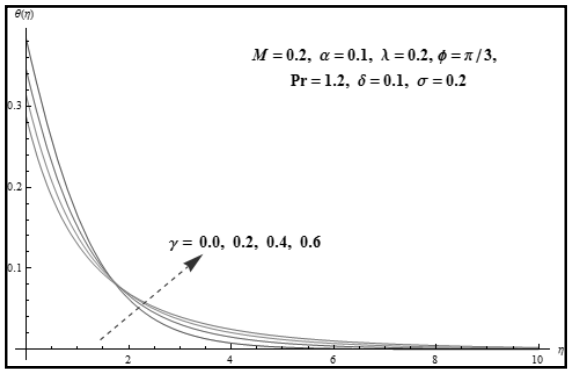

Fig. 11. Effect of γ on $\theta(\eta)$

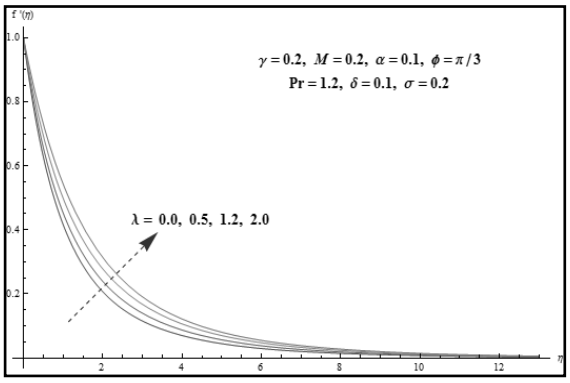

Fig. 12. Effect of λ on $f'(\eta)$

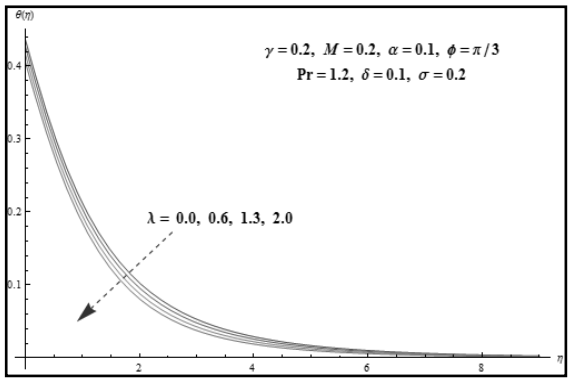

Fig. 13. Effect of λ on $\theta(\eta)$

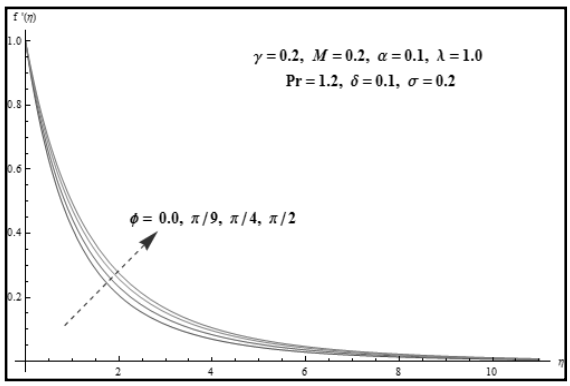

Fig. 14. Effect of φ on $f'(\eta)$

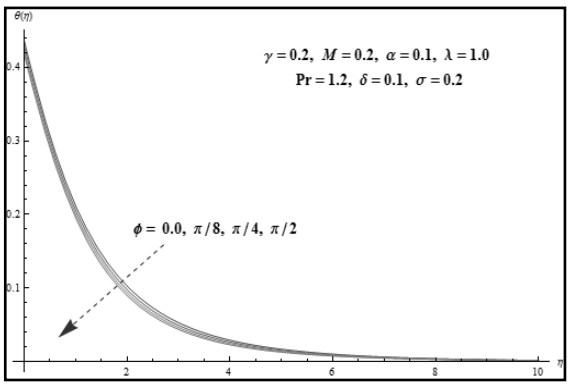

Fig. 15. Effect of φ on $\theta(\eta)$

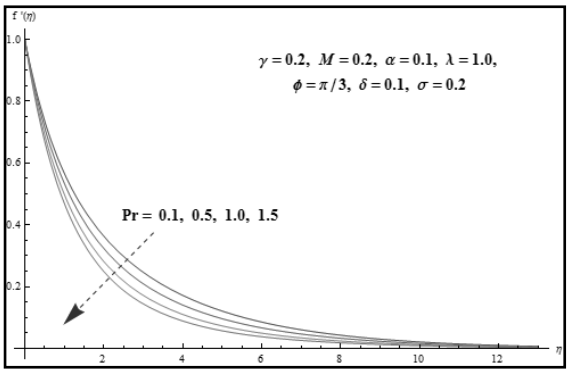

Fig. 16. Effect of Pr on $f'(\eta)$

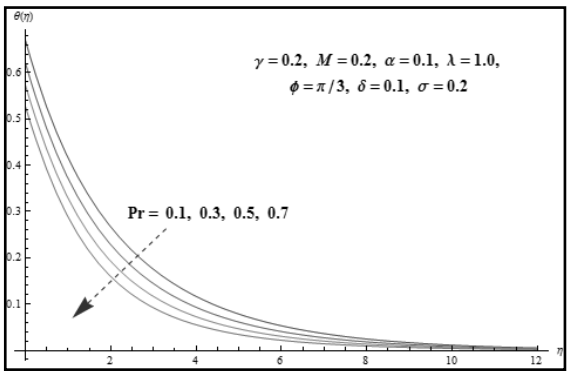

Fig. 17. Effect of Pr on $\theta(\eta)$

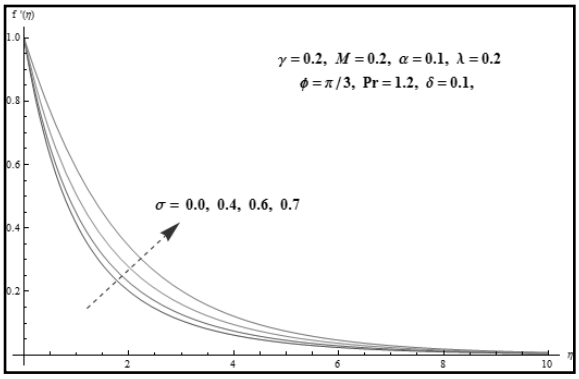

Fig. 18. Effect of σ on $f'(\eta)$

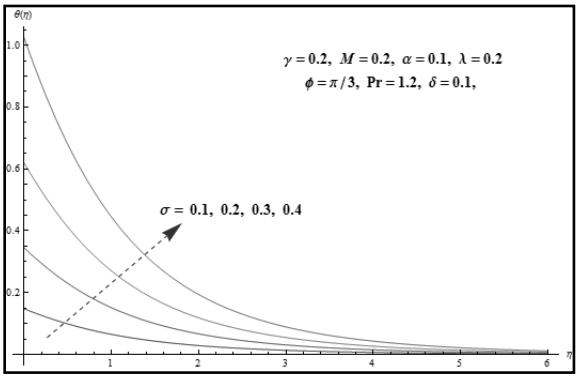

Fig. 19. Effect of σ on $\theta(\eta)$

Table 1. Convergence of the homotopy solutions for different order of approximations when $\gamma = 0.3,\ \alpha = 0.1, M = 0.2, \lambda = 0.1,\ \varphi = \pi/4, \mathrm{Pr} = 1.2, \sigma = 0.1$ and $\delta = 0.1$.

Order of approximation	$f''(0)$	$\theta'(0)$
1	–1.0563	–0.11293
5	–1.0233	–0.11642
10	–1.0192	–0.11781
15	–1.0181	–0.11835
20	–1.0181	–0.11862
23	–1.0181	–0.11873
25	–1.0181	–0.11873
30	–1.0181	–0.11873

Table 2. Skin friction coefficient $\mathrm{Re}_x^{\frac{1}{2}} C_f$ and local Nusselt number $\mathrm{Re}_x^{-\frac{1}{2}} Nu_x$ for different parameters α, γ, λ, M, δ, φ, Pr and σ.

γ	M	α	λ	φ	Pr	δ	σ	$(1+M) f''(0) - \frac{\alpha}{3} M f'''(0)$	$\sigma\left(\frac{1}{\theta(0)}+1\right)$
0	0.2	0.1	0.1	$\frac{\pi}{3}$	1.5	0.1	0.1	–1.0860	0.6752
0.2								–1.1729	0.7163
0.3								–1.2151	0.7359
0.1	0							–1.0284	0.6699
	0.2							–1.1298	0.6950
	0.4							–1.2241	0.7135
	0.2	0						–1.1314	0.6953
		0.1						–1.1298	0.6950
		0.3						–1.1264	0.6940
		0.1	0					–1.1379	0.6927
			0.1					–1.1298	0.6950
			0.3					–1.1139	0.6978
			0.1	0				–1.1379	0.6933
				$\frac{\pi}{6}$				–1.1332	0.6939
				$\frac{\pi}{3}$				–1.1298	0.6950
				$\frac{\pi}{3}$	1.3			–1.1281	0.6305
					1.5			–1.1298	0.6950
					1.6			–1.1305	0.7236
					1.5	0		–1.1316	0.8074
						0.1		–1.1298	0.6950
						0.2		–1.1261	0.5495
						0.1	0.1	–1.1298	0.6950
							0.2	–1.1186	0.6974
							0.4	–1.0761	0.7063

Table 3. Comparison of $f''(0)$ of the present values (in brackets) with the previous published results (Javed *et al*., 2013) for $\gamma = 0$ and $\lambda = 0$.

α/M	0.0	0.2	0.4	0.6	0.8	1.0
0.0	-1	-0.9131	-0.8452	-0.7906	-0.7454	-0.7071
	(-1)	(-0.912871)	(-0.845154)	(-0.790569)	(-0.745356)	(-0.707107)
0.1	-1	-0.9159	-0.8493	-0.7950	-0.7498	-0.7114
	(-1)	(-0.915896)	(-0.849293)	(-0.795027)	(-0.749789)	(-0.711366)
0.2	-1	-0.9190	-0.8536	-0.7997	-0.7544	-0.7158
	(-1)	(-0.918995)	(-0.853583)	(-0.799674)	(-0.754420)	(-0.715818)
0.3	-1	-0.9222	-0.8580	-0.8045	-0.7593	-0.7205
	(-1)	(-0.922172)	(-0.858036)	(-0.804526)	(-0.759267)	(-0.720481)
0.4	-1	-0.9254	-0.8627	-0.8096	-0.7644	-0.7254
	(-1)	(-0.925430)	(-0.862664)	(-0.809603)	(-0.764355)	(-0.725379)
0.5	-1	-0.9288	-0.8675	-0.8149	-0.7697	-0.7305
	(-1)	(-0.928774)	(-0.867484)	(-0.814928)	(-0.769707)	(-0.730534)
0.6	-1	-0.9322	-0.8725	-0.8205	-0.7754	-0.7360
	(-1)	(-0.932210)	(-0.872512)	(-0.820527)	(-0.775354)	(-0.735979)
0.7	-1	-0.9357	-0.878	-0.8264	-0.7813	-0.7418
	(-1)	(-0.935741)	(-0.877767)	(-0.826430)	(-0.781331)	(-0.741753)
0.8	-1	-0.9394	-0.8833	-0.8327	-0.7877	-0.7479
	(-1)	(-0.939375)	(-0.883271)	(-0.832675)	(-0.787681)	(-0.747883)
0.9	-1	-0.9431	-0.8891	-0.8393	-0.7954	-0.7544
	(-1)	(-0.943116)	(-0.889051)	(-0.839304)	(-0.794456)	(-0.754438)
1.0	-1	-0.9470	-0.8951	-0.8464	-0.8017	-0.7615
	(-1)	(-0.946972)	(-0.895135)	(-0.846370)	(-0.801719)	(-0.761475)

Table 4. Comparison of skin friction coefficient $\mathrm{Re}_x^{\frac{1}{2}} C_f$ of the present values (in brackets) with the previous published results (Javed *et al*., 2013) for $\gamma = 0$ and $\lambda = 0$.

α/M	0.0	0.2	0.4	0.6	0.8	1.0
0.0	-1	-1.0954	-1.1832	-1.2649	-1.3416	-1.4142
	(-1)	(-1.095445)	(-1.183216)	(-1.264911)	(-1.341641)	(-1.414214)
0.1	-1	-1.0940	-1.1808	-1.2620	-1.3384	-1.4107
	(-1)	(-1.093953)	(-1.180842)	(-1.261993)	(-1.338379)	(-1.410732)
0.2	-1	-1.0924	-1.1784	-1.2590	-1.3351	-1.4072
	(-1)	(-1.092445)	(-1.178431)	(-1.259022)	(-1.335054)	(-1.407183)
0.3	-1	1.0909	-1.1776	-1.2560	-1.3317	-1.4036
	(-1)	(-1.090921)	(-1.175981)	(-1.255996)	(-1.331665)	(-1.403562)
0.4	-1	-1.0894	-1.1735	-1.2529	-1.3282	-1.3999
	(-1)	(-1.089381)	(-1.173490)	(-1.252912)	(-1.328205)	(-1.399867)
0.5	-1	-1.0878	-1.1710	-1.2498	-1.3247	-1.3961
	(-1)	(-1.087823)	(-1.170957)	(-1.249765)	(-1.324671)	(-1.396090)
0.6	-1	-1.0862	-1.1684	-1.2466	-1.3211	-1.3922
	(-1)	(-1.086247)	(-1.168379)	(-1.246551)	(-1.321057)	(-1.392228)
0.7	-1	-1.0847	-1.1658	-1.2433	-1.3174	-1.3883
	(-1)	(-1.084653)	(-1.165752)	(-1.243267)	(-1.317359)	(-1.388272)
0.8	-1	-1.0830	-1.1631	-1.2399	-1.3136	-1.3842
	(-1)	(-1.083040)	(-1.163075)	(-1.239906)	(-1.313568)	(-1.384217)
0.9	-1	-1.0814	-1.1603	-1.2365	-1.3097	-1.3801
	(-1)	(-1.081407)	(-1.160345)	(-1.236464)	(-1.309677)	(-1.380053)
1.0	-1	-1.0798	-1.1576	-1.2329	-1.3057	-1.3758
	(-1)	(-1.079753)	(-1.157556)	(-1.232933)	(-1.305679)	(-1.375771)

4. Conclusions

In the present study we have investigated the mixed convection flow and heat transfer of Powell-Eyring fluid over an inclined stretching cylinder with Newtonian heating. The main points of our conclusion are

- Effects of M and α on velocity and temperature are quite opposite.
- Velocity and temperature of the fluid increase for higher values of curvature parameter.
- Temperature profile decreases with increase in mixed convection parameter λ and Prandtl number Pr.
- Temperature profile is higher for larger values of conjugate parameter.

References

Abbasbandy, S., Hashemi, M.S. & Hashim, I. (2013). On convergence of homotopy analysis method and its aplication to fractional integro-differential equations. Quaestiones Mathematicae, **36**:93-105.

Ara, A., Khan, N.A., Khan, H. & Sultan, F. (2014). Radiation effect on boundary layer flow of an Eyring-Powell fluid over an exponentially shrinking sheet. Ain Shams Engineering Journal, **22**:751-756.

Eldabe, N.T.M., Sallam, S.N. & Abou-zeid, M.Y. (2012). Numerical study of viscous dissipation effect on free convection heat and mass transfer of MHD non-Newtonian fluid flow through a porous medium. Journal of the Egyptian Mathematical Society, **20**:139--151.

Ferdows, M., Khan, Md. S., Alam, Md. M. & Sun, S. (2012). MHD mixed convective boundary layer flow of a nanofluid through a porous medium due to an exponentially stretching sheet. Mathematical Problems in Engineering, **2012**:408-528.

Hassan, H.N. & Rashidi, M.M. (2013). An analytical solution of micropolar fluid in a porous channel with mass injection using homotopy analysis method. International Journal of Numerical Methods for Heat & Fluid Flow, **14**(2):419-437

Hayat, T., Ashraf, M.B., Alsulami, H.H. & Alhuthali, M.S. (2014). Three-dimensional mixed convection flow of viscoelastic fluid with thermal radiation and convective conditions. PLOS ONE, **9**:e90038.

Hayat, T., Farooq, M., Alsaedi, A. & Iqbal, Z. (2013). Melting heat transfer in the stagnation point flow of Powell Eyring fluid. Journal of Thermophysics and Heat Transfer, **27**:761-766.

Jalil, M. & Asghar, S. (2013). Flow and heat transfer of Powell Eyring fluid over a stretching surface: A lie group analysis. Journal of Fluids Engineering, **135**:121201.

Javed, T., Ali, N., Abbas, Z. & Sajid, M. (2013). Flow of an Eyring-Powell Non-Newtonian Fluid over a Stretching Sheet. Chemical Engineering Communications, **200**:327-336.

Keshtkar, M.M., Esmaili, N. & Ghazanfari, M.R. (2014). Effect of heat source/sink on mHD mixed convection boundary layer flow on a vertical surface in a porous medium saturated by a nanofluid with suction or injection. Research Inventy: International Jornal of Engineering Science, **4**:1-11.

Khader, M.M. & Megahed, A.M. (2013). Numerical studies for flow and heat transfer of the Powell Eyring fluid thin film over an unsteady stretching sheet with internal heat generation using the Chebyshev finite difference method. Journal of Applied Mechanics and Technical Physics, **54**:440-450.

Li, D., Labropulu, F. & Pop, I. (2011). Mixed convection flow of a viscoelastic fluid near the orthogonal stagnation-point on a vertical surface. International Journalof Thermal Sciences, **50**:1698-1705.

Liao, S.J. (2012). Homotopy analysis method in non-linear differential equations. Springer and higher education press, Heidelberg.

Makinde, O.D. (2012). Computational modelling of MHD unsteady flow and heat transfer towards a flat plate with Navier slip and Newtonian heating. Brazilian Journal of Chemical Engineering, **29**:159-166.

Makinde, O.D. (2013). Effects of viscous dissipation and Newtonian heating on boundary layer flow of nanofluids over a flat plate. International Journal of Numerical Methods for Heat Fluids Flow, **23**:1291-1303.

Malik, M.Y., Hussain, A. & Nadeem, S. (2013). Boundary layer flow of an Eyring-Powell model fluid due to a stretching cylinder with variable viscosity. Scientia Iranica, **20**:313-321.

Merkin, J.H. (1994). Natural convection boundary layer flow on a vertical surface with Newtonian heating. International Journal of Heat and Fluid flow, **15**:392-398.

Narahari, M. & Dutta, B.K. (2012). Effects of thermal radiation and mass diffusion on free convection flow near a vertical plate with Newtonian heating. Chemical Engineering Communications, **199**:628--643.

Rashidi, M.M., Momoniat, E. & Rostami, B. (2012). Analytic approximate solutions for MHD boundary layer viscoelastic fluid flow over continuously moving stretching surface by homotopy analysis method with two auxiliary parameters. Journal of Applied Mathematics, **2012**:780415.

Sarif, N.M., Salleh, M.Z. & Nazar, R. (2013). Numerical Solution of Flow and Heat Transfer over a Stretching Sheet with Newtonian Heating using the Keller Box Method. Procedia Engineering, **53**:542-554.

Srinivasacharya, D. & Surender, O. (2014). Effect of double stratification on mixed convection boundary layer flow of a nanofluid past a vertical plate in a porous medium. Applied. Nanoscienc, **5**:29-38.

Turkyilmazoglu, M. (2012). Solution of the Thomas-Fermi equation with a convergent approach. Communications in Nonlinear Science and Numerical Simulation, **17**:4097-4103.

Uddin, M.J., Khan, W.A. & Ismail, A.I. (2012). MHD free convective boundary layer flow of a nanofluid past a flat vertical plate with Newtonian heating boundary condition. PLOS One, **7**:e49499.

Submitted **:** 17/02/2015
Revised **:** 25/08/2015
Accepted **:** 31/08/2015

إنسياب حمل مختلط لسائل باول – أيرينغ على اسطوانة مرنة تحت تأثير تسخين نيو توفي

[1]حافظ عبد الوهاب ، [2]سجاد حسين ،[2]سايرا بهاتي، [3]محمد نعيم

[1]قسم الرياضيات – جامعة الهزارة مانسيهرا – باكستان

[2]قسم الرياضيات – مجلس العموم الكندي أبوت آباد – باكستان

[3]قسم تقنية المعلومات – جامعة أبوت للعلوم والتكنولوجيا – أبوت أباد – باكستان

المقابلة المؤلف: wahabmaths@yahoo.com/wahab@hu.edu.pk

خلاصة

هدف هذا البحث هو دراسة و تحليل انسياب الحمل المختلط لسائل باول – أيرينغ الذي تحدثه اسطوانة مائلة. تحليل انتقال الحرارة يتم عبر التعرض لتسخين نيو توفي و لتوليد / امتصاص الحرارة. نستخدم التحويلات المناسبة للانتقال من نظام معادلات تفاضلية جزئية غير خطية إلى نظام معادلات تفاضلية اعتيادية . و نقوم بحل المسألة بأستخدام طريقة التحليل التحاولي. كما ننتقش سلوك الوسيطات المختلفة على معامل الاحتكاك القشري، عدد نوسلت ، السرعة ، وصور درجات الحرارة. ونعرض أخيراً مقارنة بين عامل الاحتكاك القشري للسوائل اللزجة من جهة و سوائل باول – أيرينغ من جهة أخرى ، حيث يكون لهذه السوائل معطيات متوفرة سلفاً.